A translocation causing increased α-Klotho level results in hypophosphatemic rickets and hyperparathyroidism

Catherine A. Brownstein*, Felix Adler*, Carol Nelson-Williams*, Junko Iijima[†‡], Peining Li*, Akihiro Imura[†‡], Yo-ichi Nabeshima[†‡], Miguel Reyes-Mugica[§], Thomas O. Carpenter[¶‖], and Richard P. Lifton*[‖]

*Department of Genetics, Howard Hughes Medical Institute, Yale University School of Medicine, New Haven, CT 06510; [†]Department of Pathology and Tumor Biology, Graduate School of Medicine, Kyoto University, Kyoto 606-8501, Japan; [‡]Core Research for Evolutional Science and Technology, Japan Science and Technology Corporation, Saitama 332-0012, Japan; and Departments of [§]Pathology and [¶]Pediatrics (Endocrinology), Yale University School of Medicine, New Haven, CT 06520

Contributed by Richard P. Lifton, December 30, 2007 (sent for review December 15, 2007)

Phosphate homeostasis is central to diverse physiologic processes including energy homeostasis, formation of lipid bilayers, and bone formation. Reduced phosphate levels due to excessive renal loss cause hypophosphatemic rickets, a disease characterized by prominent bone defects; conversely, hyperphosphatemia, a major complication of renal failure, is accompanied by parathyroid hyperplasia, hyperparathyroidism, and osteodystrophy. Here, we define a syndrome featuring both hypophosphatemic rickets and hyperparathyroidism due to parathyroid hyperplasia as well as other skeletal abnormalities. We show that this disease is due to a *de novo* translocation with a breakpoint adjacent to *α-Klotho*, which encodes a β-glucuronidase, and is implicated in aging and regulation of FGF signaling. Plasma α-Klotho levels and β-glucuronidase activity are markedly increased in the affected patient; unexpectedly, the circulating FGF23 level is also markedly elevated. These findings suggest that the elevated α-Klotho level mimics aspects of the normal response to hyperphosphatemia and implicate α-Klotho in the selective regulation of phosphate levels and in the regulation of parathyroid mass and function; they also have implications for the pathogenesis and treatment of renal osteodystrophy in patients with kidney failure.

bone | endocrinology | genetics | phosphorus

The maintenance of normal phosphate homeostasis is critical for diverse biochemical processes *in vivo*. Its importance is illustrated by disorders featuring hypophosphatemia due to excessive renal phosphate loss. Affected patients develop rickets, a disorder in which abnormal mineralization of bone and growth plate cartilage results in diminished bone strength, deformity, short stature, and bone pain. Rapidly growing bones of the lower extremities generally show the most striking abnormalities (1). Conversely, high phosphate levels may also have adverse physiologic effects. These are most pronounced in patients with chronic kidney disease (CKD) who develop hyperphosphatemia due to impaired renal clearance. These patients develop hyperparathyroidism and renal osteodystrophy.

The kidney plays a predominant role in the regulation of serum phosphorus levels. The vast majority of phosphate reabsorption occurs in the proximal tubule and is mediated by the sodium–phosphate cotransporter type IIa (NaPi-IIa), with additional contributions from the related protein NaPi-IIc (2, 3). Parathyroid hormone (PTH) has been considered the major regulator of NaPi-IIa and NaPi-IIc density in the proximal tubular cell apical membrane (3, 4), promoting the rapid removal of NaPi-IIa from the membrane and its subsequent degradation (5). In addition, high phosphate levels are known to promote proliferation of parathyroid cells and enhance PTH secretion and mRNA stability; these effects have been speculated to be mediated by means of reduced serum Ca^{2+} levels, but the mechanism is uncertain (6–9).

More recently, FGF23 and its receptor have been recognized to play fundamental roles in phosphate homeostasis. Homozygous loss of function mutations in FGF23 result in increased serum phosphate levels, due to increased NaPi-IIa abundance; conversely, mutations in FGF23 that increase its level by reducing degradation result in hypophosphatemia (10–12). Mutations in other genes, such as the zinc-dependent endopeptidase PHEX also result in increased FGF23 levels, renal phosphate wasting, and rickets; this is the cause of X-linked hypophosphatemic rickets (XLH) (13–15).

In mice, genetic deficiency for α-Klotho, a protein bearing β-glucuronidase activity that is found in both transmembrane and soluble forms, has received considerable attention for its effect to reduce life span. Among the phenotypes of these mice are hyperphosphatemia, enhanced renal phosphate reabsorption, and growth retardation, phenotypes similar to those seen with *FGF23* deficiency. They also have elevated serum 1,25-dihydroxyvitamin D levels due to increased expression of renal 25-hydroxyvitamin D-1-α-hydroxylase (10, 16–18). Recent studies have implicated α-Klotho in facilitating FGF receptor activation by FGF23 (19, 20) and in calcium homeostasis with *in vitro* evidence of regulation of TRPV5 in the renal distal convoluted tubule and of PTH secretion (21, 22). The role of α-Klotho in phosphate homeostasis *in vivo* and its mechanism of effect has been unclear. We describe a new human disease featuring hypophosphatemic rickets with marked parathyroid hyperplasia and demonstrate that it is caused by a mutation that results in increased levels of circulating α-Klotho.

Results

Case Report. A 13-month old girl was evaluated because of poor linear growth and increasing head size. She was the product of an uncomplicated 38-week gestation, was fed standard infant formula, and the parents were not vegetarians or participants in dietary fads. There was no history of intestinal malabsorption. Physical examination revealed a pleasant and alert infant who refused to stand. A prominent forehead, large open anterior fontanel, and knobby appearance of the wrists were present. The legs were moderately bowed, and hypertrophic physes were

Author contributions: C.A.B., F.A., C.N.-W., T.O.C., and R.P.L. designed research; C.A.B., F.A., C.N.-W., J.I., P.L., A.I., Y.-i.N., M.R.-M., and T.O.C. performed research; C.A.B., F.A., C.N.-W., P.L., M.R.-M., T.O.C., and R.P.L. analyzed data; and C.A.B., T.O.C., and R.P.L. wrote the paper.

The authors declare no conflict of interest.

Freely available online through the PNAS open access option.

[‖]To whom correspondence may be addressed. E-mail: richard.lifton@yale.edu or thomas.carpenter@yale.edu.

This article contains supporting information online at www.pnas.org/cgi/content/full/0712361105/DC1.

Table 1. Biochemical values in index case at presentation, age 7, and age 22

Parameter	Age 13 mo	Age 7 yr	Age 22 yr	Normal range
Serum PO_4^{2-}, mg/dl	2.1	2.5	1.2	4–7 (child) 2.4–4.1 (adult)
Serum Ca^{2+}, mg/dl	9.4	10.9	10.4	9.0–10.5
Serum alkaline phosphatase, units/liter	630	358	134	74–397 (child) 30–114 (adult)
Serum PTH	1,233 pg/ml N/A	N/A 81 nlEq/ml	N/A 33 nlEq/ml	50–330 pg/ml <25 nlEq/ml
Serum 1,25$(OH)_2$-vitamin D, pg/ml	59	33.3	29	20–60
Serum 25-OH-vitamin D, ng/ml	98	23.3	25	10–50
Urinary calcium/creatinine ratio, mg/mg	0.25	0.26	0.19	<0.6 (0–18 mo) <0.22 (adult)
TmP/GFR, mg/dl	1.3	N/A	0.8	>3.5

N/A, not applicable.

evident along the anterior ribs (rachitic rosary). Radiographs of the knees and wrists demonstrated florid rachitic changes of the growth plates.

The patient was assumed to have a nutritional form of rickets and was treated with 12,000 units per day of vitamin D_2, however, there was no clinical or radiographic response after several weeks. Laboratory investigations at this time revealed marked hypophosphatemia, with a serum phosphate of 2.1 mg/dl (normal 4.0–7.0). Total serum calcium was 9.4 mg/dl (normal, 9.6–11.6). Serum alkaline phosphatase activity was 630 units/liter (elevated). The serum parathyroid hormone (PTH) level was elevated, 1,233 pg/ml by C-terminal PTH assay (normal range 50–330). Other biochemical values were normal [Table 1 and supporting information (SI) Table 2]. The renal fractional excretion of phosphate was 30% (normal <15% and should be even lower in the setting of hypophosphatemia). The serum phosphorus threshold for renal phosphate wasting [i.e., the tubular threshold maximum corrected for glomerular filtration rate, or TmP/GFR (1)] was 1.3 mg/dl (normal >3.5 mg/dl), confirming inappropriate renal phosphate wasting. There was no detectable calcium in a random urine collection. Serum 25-OH-vitamin D was 98 ng/ml (elevated, reflecting the recent pharmacologic vitamin D intake) and the 1,25$(OH)_2$-vitamin D was 59 pg/ml (normal, but inappropriately so in the setting of hypophosphatemia and high 25-OH-vitamin D levels). The clinical and biochemical features were consistent with hypophosphatemic rickets due to inappropriate renal phosphate losses, and therapy was changed to 1,25$(OH)_2$-vitamin D with oral phosphate salt supplementation. Upon this treatment, her bone pain improved, and she began to walk shortly before her 2nd birthday. Radiographic examination demonstrated improvement of the epiphyseal lesions noted before therapy. Phosphate levels remained slightly below normal and were never elevated.

After several years of 1,25$(OH)_2$-vitamin D and phosphate treatment, it became evident that serum PTH levels were increasing. By age 7, the patient developed hypercalcemia, at which time she was referred to Yale Pediatric Endocrinology. At this time, her bow defect had corrected, and she had normal leg alignment. Specific features that were distinct from, or more pronounced than, those typical of the relatively common disorder XLH included macrocephaly, prominent frontal bossing, and dysplasia of the nasal bones, with exaggerated midfacial protrusion. Laboratory values revealed persistent hypophosphatemia (3.2 mg/dl) now with hypercalcemia (10.9 mg/dl, nl <10.5 mg/dl) and hyperparathyroidism (PTH level 81 nlEq/ml by midmolecule assay nl < 25). Urinary calcium/creatinine ratio (mg/mg) was 0.26. Hypercalcemia persisted despite further adjustments in the medical regimen, and surgical exploration of the neck was performed, revealing four-gland parathyroid hyperplasia; 3.5 glands were removed, with PTH values falling to 14–16 nlEq/ml. Histology revealed benign multigland hyperplasia (Fig. 1*A* and SI Fig. 6).

The patient's skeletal condition remained stable coincident with normocalcemia and hypophosphatemia until she redeveloped hypercalcemia at age 19. PTH levels were once again elevated (120–170 nlEq/ml), and repeat parathyroid surgery was performed. The one-half gland remnant had enlarged, and ≈75% of this remnant was again removed surgically, with histopathology again revealing hyperplasia (Fig. 1*B*). PTH levels fell to 3 nlEq/ml after surgery and hypophosphatemia persisted.

The patient's course has been relatively uncomplicated since that time. She has had intermittent headaches, and was found to have Arnold–Chiari 1 malformation, which has also been described in patients with XLH (23). She is now 23 years of age and has achieved an adult height of 4 feet, 11–1/2 inches (151 cm). Her leg alignment has remained normal. Her last PTH level was mildly elevated at 33 nlEq/ml (normal <25). She is functioning well as a college student.

Direct DNA sequencing of the coding regions and intron–exon splice sites of *Phex*, *FGF23*, *DMP1*, and *FGFR1* in the patient revealed only wild-type sequences, providing no evidence that mutation in these genes account for her clinical syndrome.

To search for a potential genetic explanation of the patient's syndrome, cytogenetic analysis was performed and revealed a single abnormality, a balanced translocation between chromosomes 9 and 13: t(9,13)(q21.13;q13.1) (Fig. 2). Normal karyotypes were present in both parents (who were also phenotypically normal), and genotyping confirmed biological parentage, re-

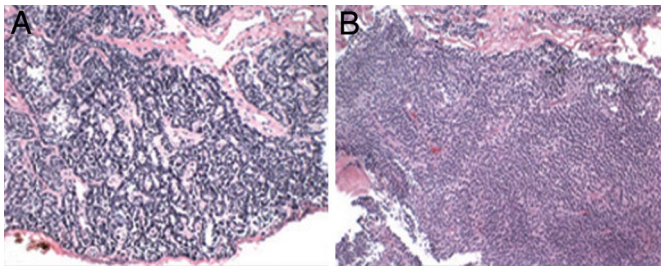

Fig. 1. Parathyroid hyperplasia in index case. (*A*) A parathyroid gland removed at the initial surgery revealed enlargement of the gland with preservation of normal trabecular architecture consistent with hyperplasia. (Original magnification, ×10). The other three glands showed similar histology. (*B*) Hyperplastic parathyroid remnant partially removed at the second surgery; findings again were consistent with parathyroid hyperplasia. (Hematoxylin–eosin stain.)

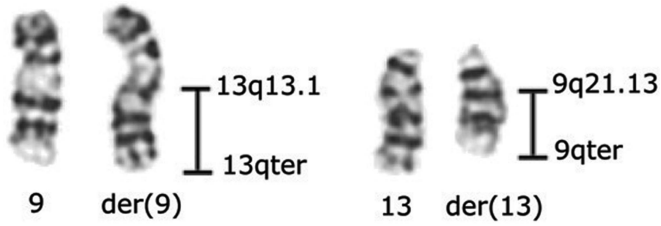

Fig. 2. A 9;13 translocation in the index case with hypophosphatemic rickets. Representative metaphase chromosomes are shown. The patient has a balanced translocation with breakpoints at 9q21.13 and 13q13.1.

vealing that the patient's translocation is *de novo*. Her unique phenotype occurring in the setting of a *de novo* chromosomal translocation implicates the translocation in the pathogenesis of the syndrome.

To map the translocation breakpoint in this patient, YAC clones spanning chromosome 13 were used to identify YACs on opposite sides of the breakpoint by fluorescent *in situ* hybridization (FISH). YACs RP11–817H3 and RP11–911F6, which lie ≈16 Mb apart, define the interval containing the chromosome 13 breakpoint. BAC clones with known positions between the flanking YACs were then mapped by FISH. BACs CTD-2336F15 and RP11–59E16, separated by 300 kb, each hybridize to two chromosomes: At one site of hybridization the fluorescent signals are concordant, marking the normal chromosome 13; the other sites are discordant, with one marking the derivative chromosome harboring proximal 13q, and the other marking the derivative chromosome harboring distal 13q (Fig. 3*A*). In the interval between these clones, we identified a BAC clone CTD–2369B11, which spans the breakpoint. This single clone hybridizes to three chromosomes, two sites that are concordant with a BAC that marks proximal chromosome 13 (one on the intact chromosome 13, one with derivative proximal chromosome 13), and a third site that marks the derivative chromosome containing distal chromosome 13. Flanking BACs to either side hybridize to only the proximal or the distal derivative of chromosome 13 (Fig. 3).

These findings indicate that the chromosome 13 translocation breakpoint occurs within the 88 kb spanned by the genomic segment of CTD–2369B11. To confirm the breakpoint and localize it more precisely, we sought restriction endonuclease cleavage products arising from the fusion of chromosome 13 and chromosome 9 sequences by Southern blotting (Fig. 4). Systematic screening using single copy probes across this interval identified a probe that marked the translocation breakpoint: It hybridized both to the expected 11.3-kb wild-type EcoRI fragment and a 8.1-kb fragment unique to the patient and absent in the genomic DNA of controls. Hybridization of the same probe to HindII-cleaved genomic DNA revealed the expected wild-type 12.3-kb fragment and an 8.5-kb fragment. Hybridization to the products of XbaI cleavage yielded only wild-type fragments. These results together indicate that the translocation breakpoint lies within the 3.5-kb interval between the last wild-type chromosome 13 XbaI site and the first anomalous EcoRI site (Fig. 4).

This translocation interval lies at position 32,435,135–32,439,970 on chromosome 13 [University of California Santa Cruz (UCSC) version hg16, National Center for Biotechnology Information (NCBI) build 34]. The DNA sequence distal to the XbaI site reveals a segment of essentially all repetitive DNA for 15 kb, which thwarted efforts to further refine the location of the breakpoint. Examination of genes in proximity to this translocation breakpoint reveals that the gene closest to the breakpoint is *α-Klotho*, whose 5′ end lies −49 kb distal to the breakpoint on chromosome 13. The closest gene proximal to the breakpoint is APRIN (androgen-induced prostate proliferative shutoff), which lies at least 429 kb proximal to the breakpoint.

An analogous approach was used to map the chromosome 9 breakpoint. BAC RP11–152I12 from chromosome 9 was found to

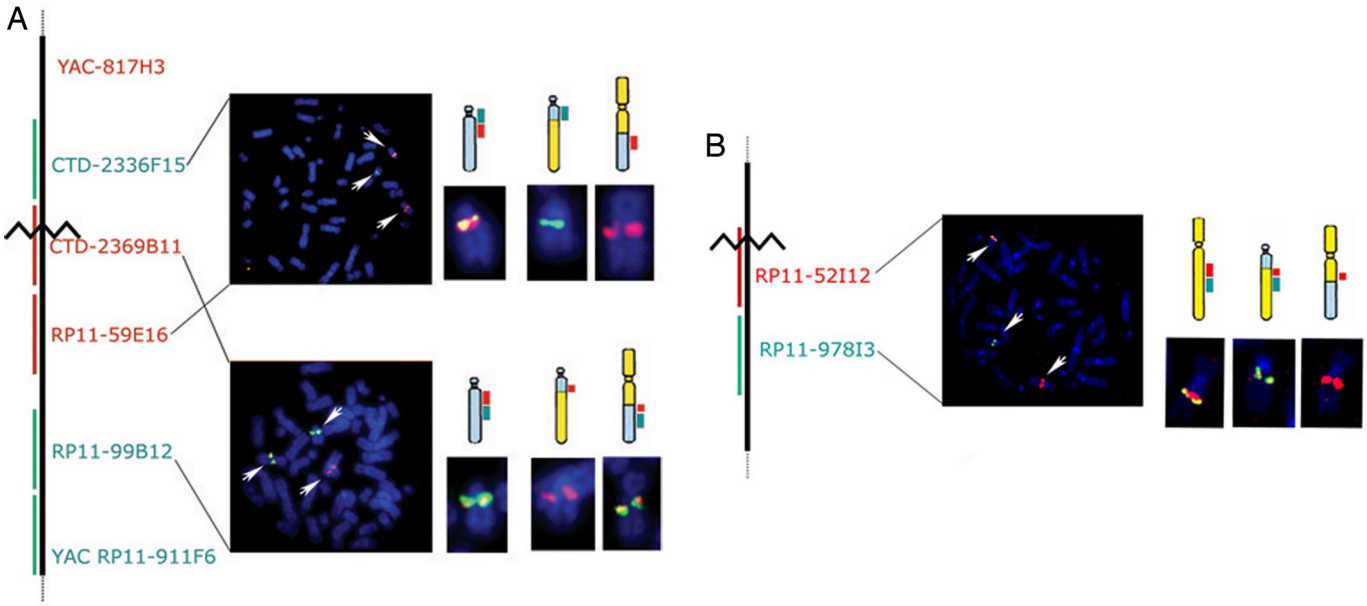

Fig. 3. Mapping breakpoints by FISH. (*A*) Mapping the chromosome 13q13.1 breakpoint. The relative position of YAC and BAC clones on chromosome 13 used in FISH experiments are shown in the schematic at the left, and the location of the inferred translocation breakpoint is indicated by the jagged line. The upper metaphase chromosome spread shows representative results of FISH using probes on opposite sides of the breakpoint. The hybridizing chromosomes are enlarged at the right, with a schematic diagram showing the signals coming from the wild-type chromosome 13 (gray) and its two derivatives. The lower spread shows the result with the spanning BAC (in red) and a distal probe, revealing three hybridization signals from the spanning BAC. (*B*) Mapping the chromosome 9q21.13 breakpoint. A representative metaphase spread in which the spanning chromosome 9 BAC and a distal marker have been hybridized. Three signals from the spanning BAC are detected.

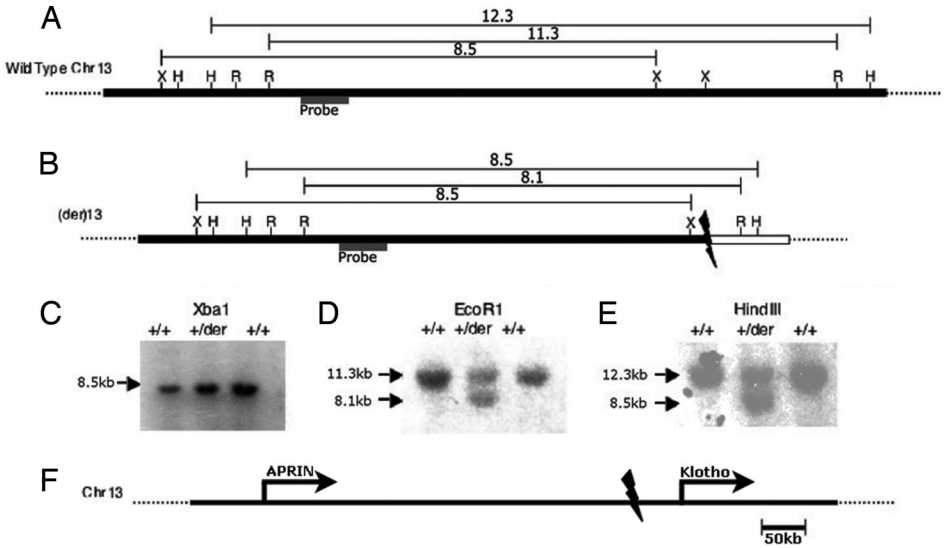

Fig. 4. Confirmation and refinement of translocation breakpoints. (*A*) A map of a segment of normal chromosome 13 spanning the inferred translocation breakpointis shown as a solid bar, and the locations of known cleavage sites for XbaI (X), HindIII (H), and EcoRI (R) are indicated. The sizes in kilobases of restriction endonuclease cleavage fragments predicted to result from Southern blotting after digestion with each enzyme and hybridization with the indicated probe are shown. (*B*) The inferred structure of the derivative chromosome is shown below, with the segment from chromosome 9 shown as a white box, along with the sizes of the observed restriction endonuclease cleavage fragment. (*C–E*) The results of Southern blotting of two control subjects (+/+) and the case (+/der) after digestion with indicated enzymes are shown. EcoRI and HindIII both yield heterozygous fragments that confirm the translocation; the normal fragments produced by XbaI delimit the proximal boundary of the translocation breakpoint. (*F*) Location of translocation breakpoint on chromosome 13. At a larger scale, the breakpoint is seen to be ≈50 kb proximal to the 5′ end of Klotho and 430 kb distal to the 3′ end of APRIN.

span the translocation breakpoint (Fig. 3*B*). The genomic segment of this BAC, RP11–152I12, is 136 kb in length and contains the 3′ end of one annotated gene, transmembrane protein 2 (TMEM2), which was not disrupted as shown by additional FISH experiments and Southern blotting (data not shown). TMEM2 is located in the autosomal recessive nonsyndromic hearing loss (ARNSHL)-linked region on chromosome 9q13–q21, and is exclusively expressed in the cochlea (24, 25). No other identified gene lies within 200 kb of the breakpoint.

Given the evidence suggesting a role for α-Klotho in phosphate homeostasis and the presence of a *de novo* translocation breakpoint adjacent to this gene, we investigated whether dysregulation of *α-Klotho* expression might cause the patient's phenotype. We measured α-Klotho protein abundance in plasma by Western blotting using specific antibodies (see *Methods*). The results show a markedly greater abundance of α-Klotho in plasma from the patient compared with that from nine age and gender-matched control subjects (Fig. 5).

α-Klotho has been shown to have beta-glucuronidase activity, which is believed to play a role in its activity *in vivo*; for example, it increases TRPV5 activity by hydrolyzing extracellular N-linked oligosaccharides, thereby stabilizing its surface expression (21). We tested whether altered total plasma β-glucuronidase activity could be detected in the patient's serum as described in *Methods*. Her plasma contained β-glucuronidase activity that was consistently higher than that of eight age- and gender-matched control subjects (mean 5-fold elevation, Fig. 5). This degree of elevation is >9 SDs removed from the matched control subjects. These findings establish that the patient's translocation is associated with a marked increase of circulating levels of α-Klotho and its associated enzymatic activity.

Because multiple hypophosphatemic states are associated with increased levels of FGF23, we considered that α-Klotho might in part act by means of a related mechanism. Indeed, circulating FGF23 levels were markedly elevated, >12-fold higher than the upper limit of normal on multiple tests (> 800 pg/ml, normal <60 pg/ml). Because calcitriol has been shown to directly increase FGF23 production (26), FGF23 levels were repeated after withdrawal of calcitriol for 7 days; the results showed persistent and unchanged elevation in FGF23 level.

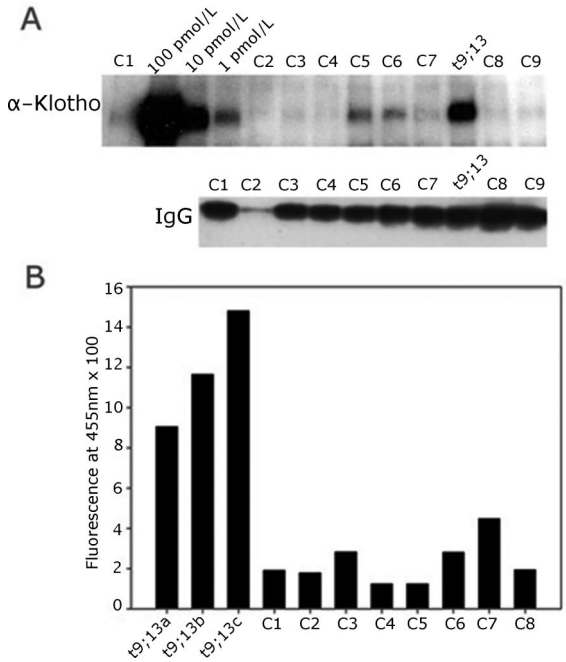

Fig. 5. Increased α-Klotho levels and activity in patient with hypophosphatemic rickets. (*A Upper*) Western blot of immunoprecipitants from serum from nine controls and the t9;13 patient for α-Klotho protein. For comparison, immunoprecipitants from 100, 10, and 1 pmol/liter recombinant human secreted α-Klotho were loaded for quantification of protein amounts. (*Lower*) Western blot of same sera probed with antibody to IgG heavy chain. (*B*) β-Glucuronidase activity in plasma of the t9;13 patient and eight age- and sex-matched controls. Levels from three independent samples from the case are compared with levels from eight age- and sex-matched controls.

Discussion

We have described a disorder featuring hypophosphatemic rickets and hyperparathyroidism due to a translocation that results in increased levels of α-Klotho. This represents an example of a mutation that causes an increase in α-Klotho activity. The inference that the translocation is the cause of the patient's syndrome is supported by the *de novo* appearance of this translocation in conjunction with the appearance of a rare syndrome, the marked alteration in α-Klotho levels in association with the mutation, and corroborating prior evidence that genetic deficiency for *α-Klotho* in mice produce the opposite phenotype (hyperphosphatemia, elevated circulating $1,25(OH)_2$-vitamin D levels and low to normal PTH (17)). In addition, during preparation of this manuscript, a likely loss of function mutation in *α-Klotho* was reported that is also associated with hyperphosphatemia, extending the prior findings from mouse to human (27). Moreover, emerging evidence indicates that α-Klotho is critical for FGF23 signaling, a regulator of renal phosphate handling (19), and also plays a role in modulating PTH secretion (22). The elevated FGF23 and PTH levels in this patient provide evidence of α-Klotho's effects on these pathways *in vivo*. We infer that the increased α-Klotho levels seen in this patient are due to a positional effect of the translocation, a mechanism well established in model systems such as *Drosophila melanogaster* (28, 29) and that plays a role in several human disease states such as Rieger syndrome (30) and holoprosencephaly (31). Importantly, mice with hypophosphatemia due to mutation in PHEX, have low Klotho levels, excluding the possibility that the observed high levels of Klotho in our patient are simply a secondary consequence of hypophosphatemia (32).

The degree of hypophosphatemia in this patient appeared to be somewhat more severe than that usually seen in X-linked hypophosphatemia (33, 34). Moreover, her distinctive facial features also distinguish her from typical patients with XLH. Hypophosphatemia was exacerbated by hyperparathyroidism but always persisted after return of PTH levels to normal after parathyroidectomy. The parathyroid hyperplasia and hyperparathyroidism in this patient is noteworthy, having thus far required two surgical procedures. Evidence of hyperparathyroidism predated phosphate treatment and progressed despite never having elevated phosphate levels, thereby excluding phosphate therapy as the cause of her hyperparathyroidism.

The present findings indicate that a primary increase in α-Klotho level is sufficient to produce hyperparathyroidism and PTH-independent hypophosphatemia. Regarding the renal phosphate wasting, α-Klotho has been shown to bind to FGF receptors and potentiate FGF23 signaling in the kidney (19, 20), and FGF23 signaling is known to be a major mediator of renal phosphate wasting. Furthermore, it is of interest that this patient's hyperparathyroidism occurs in the presence of hypophosphatemia and not the elevated phosphate levels that accompany renal failure. Moreover, α-Klotho has been reported to mediate PTH secretion *in vitro* through its maintenance of cell surface Na^+/K^+-ATPase activity (22); conversely, FGF23 has recently been shown to inhibit expression of PTH mRNA and secretion of PTH from parathyroid cells (35). Whether the elevated FGF23 level seen in our patient is the direct result of increased α-Klotho (for example, if degradation of FGF23 were prevented by interaction with α-Klotho) or is part of a negative-feedback loop responding to hyperparathyroidism is difficult to discern at present. The observation that FGF23 levels are also elevated with α-Klotho deficiency (20) suggests complex regulation of this signaling molecule.

Of further clinical relevance, the inhibition of renal phosphate reabsorption and induction of parathyroid hyperplasia in this patient resembles the normal physiologic response to chronic hyperphosphatemia. The concomitant occurrence in this patient of these two clinical findings despite persistent hypophosphatemia is consistent with a constitutive activation of the normal physiological responses to a high phosphate milieu, but in the absence of hyperphosphatemia, suggesting a role for α-Klotho in a physiologic phosphate sensing and response mechanism. Importantly, because the patient developed parathyroid hyperplasia with normal or elevated serum Ca^{2+} levels, this patient provides evidence that increased α-Klotho activity induces increased parathyroid mass without induction of hypocalcemia, the mediating step suspected to account for parathyroid hyperplasia in hyperphosphatemia. The mechanism(s) could include direct effects of α-Klotho on the parathyroid gland, with or without other factors such as reduced $1,25(OH)_2$-viamin D levels.

These findings raise a number of interesting questions for further investigation. Importantly, they support the presence of a sophisticated system for the regulation of phosphate homeostasis; the outlines of this pathway are beginning to emerge, but a number of critical pieces are as yet unknown. α-Klotho and Phex both affect FGF23 and phosphate levels; whether these gene products act in series in the same pathway or lie in independent pathways is presently unknown. Similarly, *α-Klotho* exists in both membrane-bound and soluble forms (18); the factor(s) determining this conversion and its regulation are also unknown. Most importantly, the mechanism by which altered phosphate levels are sensed and how the normal response pathway is activated is unclear. It seems unlikely that this mechanism relies on sensing of Ca^{2+} levels. It is worth noting that although *α-Klotho* was originally identified as an aging gene, it is increasingly clear that many of its primary effects concern mineral homeostasis.

Finally, these findings have potential implications for the secondary hyperparathyroidism and renal osteodystrophy that commonly develops in renal failure. These complications are believed to be promoted largely via hyperphosphatemia (36, 37). FGF23 has proven to track with PTH levels in advanced CKD, consistent either with a feedback role in response to elevated PTH levels or, alternatively, promoting PTH secretion; the molecular mechanisms of FGF23's effects on parathyroid *in vivo* have been unclear. Our findings implicate α-Klotho in the renal and parathyroid response to hyperphosphatemia and suggest that further elucidation of the details of this pathway may provide opportunities for selective therapeutic intervention that would prove efficacious in preventing renal osteodystrophy.

Methods

Human Subjects. The patient and her family members provided informed consent before enrollment in this study.

Mapping of t9;13 Breakpoint. Genomic DNA was prepared by standard methods. BAC and YAC DNAs were prepared by using Qiagen kits. Fluorescence *in situ* hybridization (FISH) was performed following manufacturer's instructions, by using chromosome 9 and 13 probes. Bacterial artificial chromosomes (BACs) were obtained from the RP11 library (BACPAC Resource Center at the Children's Hospital Oakland Research Institute, Oakland, CA) or the CTD library (Invitrogen). End-sequenced and FISH-verified BACs were selected for breakpoint mapping using the UCSC Biotechnology Genome Browser and Database (SI Table 3).

For Southern blotting, DNA was digested with indicated restriction endonucleases, fractionated via electrophoresis on 0.7% agarose gels and transferred to Hybond N+ filter membranes (Amersham). BAC probes were labeled with [α-^{32}P]dCTP by random priming or nick translation and hybridized to filters; after stringent washes, filters were exposed to film and developed. Restriction enzymes (e.g., EcoRI, BamHI, XbaI, and HindIII), and hybridization probes selected for analysis of the chromosome 13 breakpoint region and its flanking sequences were based on the July 2003 human reference sequence (UCSC version hg16, NCBI build 34) produced by the International Human Genome Sequencing Consortium.

Measurement of Serum α-Klotho Levels. Serum α-Klotho levels were determined by immunoprecipitation and Western blot analysis. Human plasma and

the standard samples were immunoprecipitated with anti-α-Klotho antibody (Mink1)-conjugated resin beads. The eluents were fractionated on 7.5% polyacrylamide gradient gels by SDS/PAGE and transferred to PVDF membranes. Blots were blocked, incubated with 10 μg/ml anti-α-Klotho (KM2076, a kind gift of Kyowa Hakko Kogyo Co.), washed, and incubated with anti-rat IgG secondary antibody. Filters were washed, and chemiluminesence was performed by using ECL+ (Amersham Pharmacia).

Measurement of α-Klotho β-glucuronidase activity was performed by adaptation of the method of Tohyama *et al.* (38), which measures the enzymatic cleavage of a synthetic β-glucuronide. The assay was performed in 100 μl of 0.5 mM 4-methylumbelliferyl (4Mu) β-D-glucuronide (Sigma), 0.1 M sodium citrate buffer (pH 5.5), 0.05 M NaCl, 0.01% Tween 20, and 20 μg of KLFc with 50 μl of fresh serum. Fluorescence intensities were measured with a DNA quantifier (μ-Quant; Bio Tek Life Sciences, with K C Junior software) at an excitation wavelength of 365 nm and an emission wavelength of 455 nm. Hydrolyzed products were quantified on the basis of 4-methylumbelliferone fluorescence. Statistical analysis was performed by using SAS software.

Measurement of Serum FGF23. Serum FGF23 levels were determined via sandwich ELISA. The ELISA for the full-length FGF23 was developed to detect only the uncleaved peptide using the combination of two monoclonal antibodies that recognize the N-terminal and the C-terminal portions, respectively, of the processing site of FGF23 (Kainos). Control samples (nine age- and sex-matched subjects) all showed values within the normal range (< 60 pg/ml).

Analysis of FGF23, PHEX, DMP1, and FGFR1 Genes. All of the coding exons of the *FGF23*, *PHEX*, *DMP1*, and *FGFR1* genes were PCR amplified by using specific primers lying in introns, 5′ or 3′ flanking noncoding regions, and directly sequenced (SI Table 4). PCR amplification carried out in a 50-μl reaction using 0.25 μM concentrations of each forward and reverse primer under the following cycle conditions: 95°C for 3 min, for 1 cycle; 95°C for 30 s, 60°C for 30 s and 72°C for 30 s, for 36 cycles; final extension 72°C for 10 min.

ACKNOWLEDGMENTS. We thank Nicole Davis, Anita Farhi, and Edward Brown for helpful discussions. This work was supported by National Institutes of Health (NIH) Clinical Investigator Award K24-HD01288 (to T.O.C.) and an NIH Center for Research Translation Award P50-AR054086 (to T.O.C.) and the Yale Clinical and Translational Science Award ULI-RR024139. R.P.L. is an investigator of the Howard Hughes Medical Institute.

1. Holm IA, *et al.* (2001) Mutational analysis and genotype-phenotype correlation of the PHEX gene in X-linked hypophosphatemic rickets. *J Clin Endocrinol Metab* 86:3889–3899.
2. Beck L, *et al.* (1998) Targeted inactivation of Npt2 in mice leads to severe renal phosphate wasting, hypercalciuria, and skeletal abnormalities. *Proc Natl Acad Sci USA* 95:5372–5377.
3. Tenenhouse H (2005) Regulation of phosphorus homeostasis by the type IIa Na/phosphate cotransporter. *Annu Rev Nutr* 25:197–214.
4. Forster IC, Hernando N, Biber J, Murer H (2006) Proximal tubular handling of phosphate: A molecular perspective. *Kidney Int* 70:1548–1559.
5. Pfister MF, *et al.* (1998) Parathyroid hormone leads to the lysosomal degradation of the renal type II Na/Pi cotransporter. *Proc Natl Acad Sci USA* 95:1909–1914.
6. Kilav R, Silver J, Naveh-Many T (2001) A conserved cis-acting element in the parathyroid hormone 3′-untranslated region is sufficient for regulation of RNA stability by calcium and phosphate. *J Biol Chem* 276:8727–8733.
7. Moallem E, Kilav R, Silver J, Naveh-Many T (1998) RNA-protein binding and post-transcriptional regulation of parathyroid hormone gene expression by calcium and phosphate. *J Biol Chem* 273:5253–5259.
8. Bell O, Silver J, Naveh-Many T (2005) Identification and characterization of cis-acting elements in the human and bovine PTH mRNA 3′-untranslated region. *J Bone Miner Res* 20:858–866.
9. Silver J, Kilav R, Sela-Brown A, Naveh-Many T (2000) Molecular mechanisms of secondary hyperparathyroidism. *Pediatr Nephrol* 14:626–628.
10. Shimada T, *et al.* FGF-23 is a potent regulator of vitamin D metabolism and phosphate homoeostasis. *J Bone Miner Res* 19:429–435.
11. Bai X, Miao D, Li J, Goltzman D, Karaplis AC (2004) Transgenic mice overexpressing human fibroblast growth factor 23(R176Q) delineate a putative role for parathyroid hormone in renal phosphate wasting disorders. *Endocrinology* 145:5269–5279.
12. Larsson T, *et al.* (2004) Transgenic mice expressing fibroblast growth factor 23 under the control of the alpha1(I) collagen promoter exhibit growth retardation, osteomalacia, and disturbed phosphate homeostasis. *Endocrinology* 145:3087–3094.
13. Sabbagh Y, Jones AO, Tenenhouse HS (2000) PHEXdb, a locus-specific database for mutations causing X-linked hypophosphatemia. *Hum Mutat* 16:1–6.
14. Guo R, Liu S, Spurney RF, Quarles LD (2001) Analysis of recombinant Phex: An endopeptidase in search of a substrate. *Am J Physiol* 281:E837–E847.
15. Jonsson KB, *et al.* (2003) Fibroblast growth factor 23 in oncogenic osteomalacia and X-linked hypophosphatemia. *N Engl J Med* 348:1656–1663.
16. Razzaque MS, Lanske B (2006) Hypervitaminosis D and premature aging: Lessons learned from Fgf23 and Klotho mutant mice. *Trends Mol Med* 12:298–305.
17. Kuro-o M, *et al.* (1997) Mutation of the mouse klotho gene leads to a syndrome resembling ageing. *Nature* 390:45–51.
18. Matsumura Y, *et al.* (1998) Identification of the human klotho gene and its two transcripts encoding membrane and secreted klotho protein. *Biochem Biophys Res Commun* 242:626–630.
19. Kurosu H, *et al.* (2006) Regulation of fibroblast growth factor-23 signaling by klotho. *J Biol Chem* 281:6120–6123.
20. Urakawa I, *et al.* (2006) Klotho converts canonical FGF receptor into a specific receptor for FGF23. *Nature* 444:770–774.
21. Chang Q, *et al.* (2005) The β-glucuronidase klotho hydrolyzes and activates the TRPV5 channel. *Science* 310:490–493.
22. Imura A, *et al.* (2007) α-Klotho as a regulator of calcium homeostasis. *Science* 316:1615–1618.
23. Caldemeyer KS, *et al.* (1995) Chiari malformation: Association with hypohosphatemic rickets and MR imaging appearance. *Radiology* 195:602–604.
24. Scott DA, *et al.* (2000) Refining the DFNB7-DFNB11 deafness locus using intragenic polymorphisms in a novel gene, TMEM2. *Gene* 246:265–274.
25. Guo J, Cheng H, Zhao S, Yu L (2006) GG: A domain involved in phage LTF apparatus and implicated in human MEB and non-syndromic hearing loss diseases. *FEBS Lett* 580:581–584.
26. Nishi H, *et al.* (2005) Intravenous calcitriol therapy increases serum concentrations of fibroblast growth factor-23 in dialysis patients with secondary hyperparathyroidism. *Nephron* 101:c94–c99.
27. Ichikawa S, *et al.* (2007) A homozygous missense mutation in human KLOTHO causes severe tumoral calcinosis. *J Clin Invest* 117:2684–2691.
28. Qumsiyeh MB (1999) Structure and function of the nucleus: Anatomy and physiology of chromatin. *Cell Mol Life Sci* 55:1129–1140.
29. Gerasimova TI, Gdula DA, Gerasimov DV, Simonova O, Corces VG (1995) A *Drosophila* protein that imparts directionality on a chromatin insulator is an enchacer of position-effect variegation. *Cell* 82:587–597.
30. Datson NA, *et al.* (1996) Closing in on the Rieger syndrome gene on 4q25: Mapping translocation breakpoints within a 50-kb region. *Am J Hum Genet* 59:1297–1305.
31. Fernandez BA, Siegel-Bartelt J, Herbrick JA, Teshima I, Scherer SW (2005) Holoprosencephaly and cleidocranial dysplasia in a patient due to two position-effect mutations: Case report and review of the literature. *Clin Genet* 68:349–359.
32. Meyer MH, Dulde E, Meyer RA, Jr (2004) The genomic response of the mouse kidney to low-phosphate diet is altered in X-linked hypophosphatemia. *Physiol Genom* 18:4–11.
33. Seikaly MG, Quigley R, Baum M (2000) Effect of dipyridamole on serum and urinary phosphate in X-linked hypophosphatemia. *Pediatr Nephrol* 15:57–59.
34. Carpenter T (1997) New perspectives on the biology and treatment of X-linked hypophosphatemic rickets. *Pediatr Clin North Am* 44:433–466.
35. Krajisnik T, *et al.* (2007) Fibroblast growth factor-23 regulates parathyroid hormone and 1α-hydroxylase expression in cultured bovine parathyroid cells. *J Endocrinol* 195:125–131
36. Hruska KA, Saab G, Mathew S, Lund R (2007) Renal osteodystrophy, phosphate homeostasis, and vascular calcification. *Semin Dial* 20:309–315.
37. Cozzolino M, Gallieni M, Chiarelli G, Brancaccio D (2006) Calcium and phosphate handling in peritoneal dialysis. *Contrib Nephrol* 150:214–225.
38. Tohyama O, *et al.* (2004) Klotho is a novel β-glucuronidase capable of hydrolyzing steroid β-glucuronides. *J Biol Chem* 279:9777–9784.